https://doi.org/10.1016/j.jsv.2021.116176

To: Journal of Sound and Vibration

Dynamic condensation approach for response-based finite element model updating of large-scale structures

Wei Tian
Department of Civil and Environmental Engineering,
The Hong Kong Polytechnic University,
Hung Hom, Kowloon, Hong Kong
cewei.tian@connect.polyu.hk

Shun Weng
Professor,
School of Civil and Hydraulic Engineering,
Huazhong University of Science and Technology,
Wuhan, Hubei, P. R. China
wengshun@hust.edu.cn

Qi Xia
School of Civil Engineering,
Southeast University,
Nanjing, Jiangsu, P. R. China
qixia@seu.edu.cn

Yong Xia*
Professor,
Department of Civil and Environmental Engineering,
The Hong Kong Polytechnic University,
Hung Hom, Kowloon, Hong Kong
ceyxia@polyu.edu.hk

(* Corresponding author)

Abstract

This study develops the dynamic condensation approach to improve the computational efficiency of response-based finite element model updating of large-scale structures. Using the dynamic condensation approach, a small number of degrees of freedom (DOFs) are selected as master DOFs. A transformation matrix is then derived to relate the master DOFs to the total DOFs. The global vibration equation is reduced into a much smaller one by using the transformation matrix. The responses are calculated efficiently from the reduced vibration equation. The response sensitivities are derived directly from the reduced vibration equation to ensure that the response sensitivities with respect to design parameters are calculated simultaneously and efficiently. The response-based model updating is then performed using a few time history responses and response sensitivities only. The computational precision and efficiency of the proposed model updating method are verified using a steel frame and a large-scale suspension bridge.

Keywords: Model updating; Dynamic condensation approach; Structural responses; Response sensitivities

1. Introduction

Model updating is widely used in damage detection and structural health monitoring [1-4]. It adjusts certain parameters of the finite element (FE) model of a structure iteratively in an optimal to ensure the analytical dynamic properties of the model match the corresponding tested data. The discrepancies between the tested data and the analytical counterparts are usually used to construct an objective function, which is then minimized with optimization algorithms. Sensitivity-based methods calculate the sensitivity matrix of the objective function with respect to the updating parameters, thereby providing a rapid optimal searching direction. They are computationally efficient for large-scale structures with numerous degrees of freedom (DOFs) and design parameters and are thus widely used in model updating of practical structures [5]. Recently, various stochastic optimization methods have also been developed to handle the local optimum of complex problems [6-12]. These methods use random searching operators to escape local optimum at the expense of increased computational costs and function evaluation times.

Modal-based model updating methods construct the objective function by using natural frequencies and mode shapes or their derivative modal features, such as the modal strain energy, modal flexibility, and strain mode shape [13-17]. The modal-based model updating methods utilize the modal characteristics extracted from the measured response data, which inherently introduce errors and lose some high-frequency modal information [18, 19]. Moreover, detecting and quantifying the localized minor elemental changes with the low-frequency modal

data are difficult. The response-based methods, which usually use measured time history responses directly for model updating, can avoid the extraction errors and retain high-frequency modal information. Therefore, much fewer measured points and short time histories are sufficient for accurate model updating. Link and Weiland [19] compared the modal-based and response-based model updating methods for the damage detection results of a layered test beam. They discovered that the response-based method could detect the structural damages clearly with only five measured points even if the analytical responses were subjected to artificial errors of damping and modal truncation errors; however, 86 measured points are required for the modal-based method. Fu et al. [20] developed a response sensitivity-based model updating method to identify local damages of plate structures by using short time histories of a few measured points.

However, the response-based model updating is seldom used in large-scale structures because of computational problems. In the response-based methods, the structural responses are usually calculated using numerical time integration methods, such as Newmark-β method and Wilson-θ method. The response sensitivities are computed in terms of the derivatives of the structural responses with respect to the design parameters using the finite difference method [21], perturbation method [22], adjoint structure method [23], and direct differentiation method [24]. These methods compute the structural responses and response sensitivities in the global structure level, which is very time-consuming when a large-scale structure with numerous DOFs and design parameters and many time steps are concerned.

Dynamic condensation approach is effective to deal with large-size problems. It selects a small number of structural DOFs as master DOFs. A transformation matrix is then derived to relate the master DOFs to the other DOFs (slave DOFs). A reduced system of much smaller size is formed using the transformation matrix. Vibration analysis performed on the reduced system saves considerable computational time. Guyan [25] firstly proposed a static condensation technique to reduce the system mass and stiffness matrices. Friswell et al. [26, 27] extended it to dynamic analysis with an iterated improved reduced system, which is known as the dynamic condensation approach. The method was subsequently improved by Xia and Lin [28, 29] to achieve much faster convergence of eigensolutions. Qu and Selvam [30] proposed an accelerated iterative dynamic condensation approach for model order reduction of viscously damped vibration systems. Lima et al. [31] addressed a time domain condensation strategy for viscoelastic linear and nonlinear systems. Mercer et al. [32] studied the effects of sensor placement on the quality of Guyan condensation method and improved the computational accuracy by using sensor optimization techniques. Kim et al. [33] integrated the free-interface substructuring method with the dynamic condensation method to handle relatively large and more complex structures efficiently. As the selection of master DOFs is closely related to the accuracy and efficiency of dynamic condensation methods, Jeong et al. [34] proposed a rational master DOFs selection method via energy distribution matrices. Yin and Zhu [35] interpreted measured data with Bayesian inference to select master DOFs for dynamic reduction-based damage detection methods optimally. Weng et al. [36, 37] developed the dynamic condensation approach to compute eigensensitivities and response sensitivities of large-scale structures efficiently.

This paper develops the dynamic condensation approach to improve the computational accuracy and efficiency of response-based FE model updating of large-scale structures. The dynamic condensation approach is used to transform the global vibration equation into a reduced one with a much smaller size. The structural responses are calculated efficiently from the reduced vibration equation with numerical time integration methods. The response sensitivities are derived directly from the reduced vibration equation without additional master DOFs used in our previous study [37]; thus, the computational efficiency of response sensitivities is improved greatly. The time history responses and response sensitivities at a few measurement points are then used for model updating. The accuracy and efficiency of the proposed model updating method are verified using a steel frame model and a long-span suspension bridge model.

2. Dynamic condensation approach for responses and response sensitivities

In the response-based FE model updating, structural responses are often used to form the objective function, and the response sensitivities are used to indicate the optimal searching direction. In the present study, the dynamic condensation approach is used for fast computation of the structural responses and response sensitivities.

2.1 Responses

The vibration equation of a structure with N DOFs is expressed as

$$\mathbf{M}\ddot{\mathbf{x}}(t)+\mathbf{C}\dot{\mathbf{x}}(t)+\mathbf{K}\mathbf{x}(t)=\mathbf{F}(t) \tag{1}$$

where **M**, **C** and **K** are the mass, damping and stiffness matrices of the structure, respectively; $\ddot{\mathbf{x}}(t)$, $\dot{\mathbf{x}}(t)$ and $\mathbf{x}(t)$ are the structural acceleration, velocity and displacement responses, respectively, at time step t; $\mathbf{F}(t)$ is the external force imposed on the structure at time step t. The Rayleigh damping $\mathbf{C} = a\mathbf{M} + b\mathbf{K}$ is used, where a and b are the damping coefficients with respect to the mass and stiffness matrices, respectively. The time variable t is omitted hereinafter for brevity.

In the dynamic condensation approach, all DOFs of the global structure are divided into master and slave ones. A time-invariant transformation matrix **T** is used to relate the structural responses of all DOFs to the master ones as [37]

$$\mathbf{x}=\mathbf{T}\mathbf{x}_m=\begin{Bmatrix}\mathbf{x}_m\\ \mathbf{x}_s\end{Bmatrix},\ \dot{\mathbf{x}}=\mathbf{T}\dot{\mathbf{x}}_m=\begin{Bmatrix}\dot{\mathbf{x}}_m\\ \dot{\mathbf{x}}_s\end{Bmatrix},\ \ddot{\mathbf{x}}=\mathbf{T}\ddot{\mathbf{x}}_m=\begin{Bmatrix}\ddot{\mathbf{x}}_m\\ \ddot{\mathbf{x}}_s\end{Bmatrix} \tag{2}$$

where subscripts 'm' and 's' denote variables associated with the master and slave DOFs, respectively. Assuming that the numbers of master and slave DOFs are N_m and N_s, respectively, $N = N_m + N_s$ and $N_m << N$. The transformation matrix **T** has the size of $N \times N_m$.

Substituting Eq. (2) into Eq. (1) and premultiplying both sides of Eq. (1) by $\mathbf{T}^{\mathrm{T}}$ leads to

$$\mathbf{M}_R\ddot{\mathbf{x}}_m+\mathbf{C}_R\dot{\mathbf{x}}_m+\mathbf{K}_R\mathbf{x}_m=\mathbf{F}_R \tag{3}$$

where $\mathbf{M}_R$, $\mathbf{C}_R$, $\mathbf{K}_R$ and $\mathbf{F}_R$ are the mass, damping, stiffness and excitation matrices of the reduced system, respectively. They are expressed as

$$\mathbf{M}_R=\mathbf{T}^{\mathrm{T}}\mathbf{M}\mathbf{T} \tag{4}$$

$$\mathbf{K}_R=\mathbf{T}^{\mathrm{T}}\mathbf{K}\mathbf{T} \tag{5}$$

$$\mathbf{C}_R = \mathbf{T}^{\mathrm{T}}\mathbf{C}\mathbf{T} = a\mathbf{M}_R + b\mathbf{K}_R \tag{6}$$

$$\mathbf{F}_R = \mathbf{T}^{\mathrm{T}}\mathbf{F} \tag{7}$$

where superscript 'T' denotes the matrix transpose. Eq. (3) is the reduced vibration equation in the order of N_m, which is much smaller than the original global vibration equation Eq. (1) of N. The calculation of structural responses based on Eq. (3) saves plenty of computational time and resources.

The primary task of dynamic condensation is to compute the transformation matrix **T**, which is a constant matrix for a linear system, indicating the inherent physical relationship between the master and total DOFs. The free vibration system shares the same **T** as the damped and force vibration case [37]. The free vibration case of Eq. (1) is expressed in a block form in terms of the master and slave DOFs as

$$\begin{bmatrix} \mathbf{M}_{mm} & \mathbf{M}_{ms} \\ \mathbf{M}_{ms}^{\mathrm{T}} & \mathbf{M}_{ss} \end{bmatrix} \begin{Bmatrix} \ddot{\mathbf{x}}_m \\ \ddot{\mathbf{x}}_s \end{Bmatrix} + \begin{bmatrix} \mathbf{K}_{mm} & \mathbf{K}_{ms} \\ \mathbf{K}_{ms}^{\mathrm{T}} & \mathbf{K}_{ss} \end{bmatrix} \begin{Bmatrix} \mathbf{x}_m \\ \mathbf{x}_s \end{Bmatrix} = \mathbf{0} \tag{8}$$

The second line of Eq. (8) provides

$$\mathbf{x}_s = -\mathbf{K}_{ss}^{-1}\left(\mathbf{M}_{ms}^{\mathrm{T}}\ddot{\mathbf{x}}_m + \mathbf{M}_{ss}\ddot{\mathbf{x}}_s + \mathbf{K}_{ms}^{\mathrm{T}}\mathbf{x}_m\right) \tag{9}$$

By substituting Eq. (9) into Eq. (2), one can obtain

$$\mathbf{x} = \mathbf{T}\mathbf{x}_m = \begin{Bmatrix} \mathbf{x}_m \\ \mathbf{x}_s \end{Bmatrix} = \begin{bmatrix} \mathbf{I}_m \\ -\mathbf{K}_{ss}^{-1}\mathbf{K}_{ms}^{\mathrm{T}} \end{bmatrix} \mathbf{x}_m - \begin{bmatrix} \mathbf{0} \\ \mathbf{K}_{ss}^{-1} \end{bmatrix} \begin{bmatrix} \mathbf{0} & \mathbf{0} \\ \mathbf{M}_{ms}^{\mathrm{T}} & \mathbf{M}_{ss} \end{bmatrix} \mathbf{T}\ddot{\mathbf{x}}_m = \mathbf{T}_G\mathbf{x}_m - \mathbf{S}\tilde{\mathbf{M}}\mathbf{T}\ddot{\mathbf{x}}_m \tag{10}$$

where

$$\mathbf{T}_G = \begin{bmatrix} \mathbf{I}_m \\ -\mathbf{K}_{ss}^{-1}\mathbf{K}_{ms}^{\mathrm{T}} \end{bmatrix} \tag{11}$$

$$\mathbf{S} = \begin{bmatrix} \mathbf{0} \\ \mathbf{K}_{ss}^{-1} \end{bmatrix} \tag{12}$$

$$\tilde{\mathbf{M}} = \begin{bmatrix} \mathbf{0} & \mathbf{0} \\ \mathbf{M}_{ms}^{\mathrm{T}} & \mathbf{M}_{ss} \end{bmatrix} \tag{13}$$

where $\mathbf{I}_m$ is a unity matrix in the order of N_m, and $\mathbf{T}_G$ is equivalent to the transformation matrix in the Guyan static condensation method [25].

Similarly, the free vibration equation of the condensed system is expressed as

$$\mathbf{M}_R \ddot{\mathbf{x}}_m + \mathbf{K}_R \mathbf{x}_m = \mathbf{0} \tag{14}$$

Eq. (14) can be simplified as [37]

$$\mathbf{M}_d \ddot{\mathbf{x}}_m + \mathbf{K}_G \mathbf{x}_m = \mathbf{0} \tag{15}$$

where

$$\mathbf{M}_d = \mathbf{T}_G^{\mathrm{T}} \mathbf{M} \mathbf{T} \tag{16}$$

$$\mathbf{K}_G = \mathbf{T}_G^{\mathrm{T}} \mathbf{K} \mathbf{T}_G \tag{17}$$

Derivation and convergence of Eq. (15) can be found in Refs. [28] and [37].

Eq. (15) is rewritten as

$$\ddot{\mathbf{x}}_m = -\mathbf{M}_d^{-1} \mathbf{K}_G \mathbf{x}_m \tag{18}$$

Substituting Eq. (18) into Eq. (10) leads to

$$\mathbf{T} = \mathbf{T}_G + \mathbf{S}\tilde{\mathbf{M}}\mathbf{T}\mathbf{M}_d^{-1}\mathbf{K}_G \tag{19}$$

Eqs. (16) and (19) present an iterative process to compute the transformation matrix $\mathbf{T}$. Once $\mathbf{T}$ is available, the reduced system matrices $\mathbf{M}_R$, $\mathbf{K}_R$, $\mathbf{C}_R$ and $\mathbf{F}_R$ are calculated from Eqs. (4)–(7). The structural responses at master DOFs $\ddot{\mathbf{x}}_m$, $\dot{\mathbf{x}}_m$ and $\mathbf{x}_m$ are calculated efficiently from the reduced vibration equation (Eq. (3)) with numerical time integration methods. The

structural responses at all DOFs $\ddot{\mathbf{x}}$, $\dot{\mathbf{x}}$ and $\mathbf{x}$ are finally recovered by those of the master DOFs from Eq. (2).

2.2 Response sensitivities

Differentiating Eq. (3) with respect to the design parameter *r* provides

$$\mathbf{M}_R \frac{\partial \ddot{\mathbf{x}}_m}{\partial r} + \mathbf{C}_R \frac{\partial \dot{\mathbf{x}}_m}{\partial r} + \mathbf{K}_R \frac{\partial \mathbf{x}_m}{\partial r} = \frac{\partial \mathbf{F}_R}{\partial r} - \frac{\partial \mathbf{M}_R}{\partial r} \ddot{\mathbf{x}}_m - \frac{\partial \mathbf{C}_R}{\partial r} \dot{\mathbf{x}}_m - \frac{\partial \mathbf{K}_R}{\partial r} \mathbf{x}_m \tag{20}$$

The derivative matrices of the reduced system $\frac{\partial \mathbf{M}_R}{\partial r}$, $\frac{\partial \mathbf{K}_R}{\partial r}$, $\frac{\partial \mathbf{C}_R}{\partial r}$ and $\frac{\partial \mathbf{F}_R}{\partial r}$ are calculated by differentiating Eqs. (4)–(7) with respect to *r* as

$$\frac{\partial \mathbf{M}_R}{\partial r} = \frac{\partial \mathbf{T}^{\mathrm{T}}}{\partial r} \mathbf{M}\mathbf{T} + \mathbf{T}^{\mathrm{T}} \frac{\partial \mathbf{M}}{\partial r} \mathbf{T} + \mathbf{T}^{\mathrm{T}} \mathbf{M} \frac{\partial \mathbf{T}}{\partial r} \tag{21}$$

$$\frac{\partial \mathbf{K}_R}{\partial r} = \frac{\partial \mathbf{T}^{\mathrm{T}}}{\partial r} \mathbf{K}\mathbf{T} + \mathbf{T}^{\mathrm{T}} \frac{\partial \mathbf{K}}{\partial r} \mathbf{T} + \mathbf{T}^{\mathrm{T}} \mathbf{K} \frac{\partial \mathbf{T}}{\partial r} \tag{22}$$

$$\frac{\partial \mathbf{C}_R}{\partial r} = a \frac{\partial \mathbf{M}_R}{\partial r} + b \frac{\partial \mathbf{K}_R}{\partial r} \tag{23}$$

$$\frac{\partial \mathbf{F}_R}{\partial r} = \frac{\partial \mathbf{T}^{\mathrm{T}}}{\partial r} \mathbf{F} \tag{24}$$

Since the response sensitivities are usually calculated together with the structural responses, many intermediate variables generated in the calculation of structural responses can be reused directly, such as $\mathbf{M}_R$, $\mathbf{C}_R$, $\mathbf{K}_R$, $\ddot{\mathbf{x}}_m$, $\dot{\mathbf{x}}_m$, $\mathbf{x}_m$ and $\mathbf{T}$. $\frac{\partial \mathbf{M}}{\partial r}$ and $\frac{\partial \mathbf{K}}{\partial r}$ are the specific elemental mass and stiffness matrices associated with the design parameter *r*, which can be calculated directly. Therefore, only $\frac{\partial \mathbf{T}}{\partial r}$ is unknown in Eqs. (21)–(24) to compute $\frac{\partial \mathbf{M}_R}{\partial r}$, $\frac{\partial \mathbf{K}_R}{\partial r}$, $\frac{\partial \mathbf{C}_R}{\partial r}$ and $\frac{\partial \mathbf{F}_R}{\partial r}$.

In our previous method [37], the design parameter *r* is localized within the master DOFs by selecting the DOFs associated with *r* as additional master DOFs to simplify the computation

of $\frac{\partial \mathbf{T}}{\partial r}$. This method is efficient to compute the response sensitivities associated with only a few design parameters but ineffective for model updating when all design parameters are concerned in a large-scale structure. To improve the computational efficiency of model updating, $\frac{\partial \mathbf{T}}{\partial r}$ is derived here directly without the additional master DOFs. As $\mathbf{T}$ is estimated through an iterative process from Eqs. (16) and (19), $\frac{\partial \mathbf{T}}{\partial r}$ can be calculated iteratively according to the derivatives of Eqs. (16) and (19) with respect to r as

$$\frac{\partial \mathbf{M}_d}{\partial r} = \frac{\partial \mathbf{T}_G^{\mathrm{T}}}{\partial r}\mathbf{M}\mathbf{T} + \mathbf{T}_G^{\mathrm{T}}\frac{\partial \mathbf{M}}{\partial r}\mathbf{T} + \mathbf{T}_G^{\mathrm{T}}\mathbf{M}\frac{\partial \mathbf{T}}{\partial r} \tag{25}$$

$$\frac{\partial \mathbf{T}}{\partial r} = \frac{\partial \mathbf{T}_G}{\partial r} + \left(\frac{\partial \mathbf{S}}{\partial r}\tilde{\mathbf{M}}\mathbf{T} + \mathbf{S}\frac{\partial \tilde{\mathbf{M}}}{\partial r}\mathbf{T} + \mathbf{S}\tilde{\mathbf{M}}\frac{\partial \mathbf{T}}{\partial r}\right)\mathbf{M}_d^{-1}\mathbf{K}_G + \mathbf{S}\tilde{\mathbf{M}}\mathbf{T}\mathbf{M}_d^{-1}\left(\frac{\partial \mathbf{K}_G}{\partial r} - \frac{\partial \mathbf{M}_d}{\partial r}\mathbf{M}_d^{-1}\mathbf{K}_G\right) \tag{26}$$

where

$$\frac{\partial \mathbf{T}_G}{\partial r} = \begin{bmatrix} \mathbf{0} \\ \mathbf{K}_{ss}^{-1}\dfrac{\partial \mathbf{K}_{ss}}{\partial r}\mathbf{K}_{ss}^{-1}\mathbf{K}_{ms}^{\mathrm{T}} - \mathbf{K}_{ss}^{-1}\dfrac{\partial \mathbf{K}_{ms}^{\mathrm{T}}}{\partial r} \end{bmatrix} \tag{27}$$

$$\frac{\partial \mathbf{S}}{\partial r} = \begin{bmatrix} \mathbf{0} \\ -\mathbf{K}_{ss}^{-1}\dfrac{\partial \mathbf{K}_{ss}}{\partial r}\mathbf{K}_{ss}^{-1} \end{bmatrix} \tag{28}$$

$$\frac{\partial \tilde{\mathbf{M}}}{\partial r} = \begin{bmatrix} \mathbf{0} & \mathbf{0} \\ \dfrac{\partial \mathbf{M}_{ms}^{\mathrm{T}}}{\partial r} & \dfrac{\partial \mathbf{M}_{ss}}{\partial r} \end{bmatrix} \tag{29}$$

$$\frac{\partial \mathbf{K}_G}{\partial r} = \frac{\partial\left(\mathbf{T}_G^{\mathrm{T}}\mathbf{K}\mathbf{T}_G\right)}{\partial r} = \frac{\partial \mathbf{T}_G^{\mathrm{T}}}{\partial r}\mathbf{K}\mathbf{T}_G + \mathbf{T}_G^{\mathrm{T}}\frac{\partial \mathbf{K}}{\partial r}\mathbf{T}_G + \mathbf{T}_G^{\mathrm{T}}\mathbf{K}\frac{\partial \mathbf{T}_G}{\partial r} \tag{30}$$

After $\frac{\partial \mathbf{T}}{\partial r}$ is obtained, $\frac{\partial \mathbf{M}_R}{\partial r}$, $\frac{\partial \mathbf{K}_R}{\partial r}$, $\frac{\partial \mathbf{C}_R}{\partial r}$ and $\frac{\partial \mathbf{F}_R}{\partial r}$ are computed from Eqs. (21)–(24). The response sensitivities at master DOFs $\frac{\partial \ddot{\mathbf{x}}_m}{\partial r}$, $\frac{\partial \dot{\mathbf{x}}_m}{\partial r}$ and $\frac{\partial \mathbf{x}_m}{\partial r}$ are calculated by applying numerical time integration methods to Eq. (20).

The dynamic condensation approach derives the response sensitivities based on the small-sized reduced system, which can save considerable computational time and resources compared with the traditional method performed on the global system. The response sensitivities at all DOFs are recovered by those at master DOFs as

$$\frac{\partial \ddot{\mathbf{x}}}{\partial r}=\frac{\partial \mathbf{T}}{\partial r}\ddot{\mathbf{x}}_m+\mathbf{T}\frac{\partial \ddot{\mathbf{x}}_m}{\partial r},\frac{\partial \dot{\mathbf{x}}}{\partial r}=\frac{\partial \mathbf{T}}{\partial r}\dot{\mathbf{x}}_m+\mathbf{T}\frac{\partial \dot{\mathbf{x}}_m}{\partial r},\frac{\partial \mathbf{x}}{\partial r}=\frac{\partial \mathbf{T}}{\partial r}\mathbf{x}_m+\mathbf{T}\frac{\partial \mathbf{x}_m}{\partial r} \tag{31}$$

As the response sensitivities are derived directly without additional master DOFs, the master DOFs remain unchanged for the response sensitivities associated with different design parameters. The intermediate variables obtained in the calculation of structural responses can be shared to compute response sensitivities with respect to different design parameters. Thus, the computational efficiency is improved greatly. The proposed method is promising to be very efficient to cope with large-scale structures with numerous design parameters given that the calculation of the response sensitivities consumes the majority of the computational time in model updating, which will be demonstrated later in the case studies.

3. Response-based FE model updating using dynamic condensation approach

In response-based FE model updating, an objective function is constructed from the weighted discrepancies between the experimental and analytical responses as

$$f(r)=\mathbf{W}\left\{\mathbf{X}^A(r)-\mathbf{X}^E\right\}+\beta\|r\|_1 \tag{32}$$

where $\mathbf{X}^E=\left\{\ddot{\mathbf{x}}^E \quad \dot{\mathbf{x}}^E \quad \mathbf{x}^E\right\}^{\mathrm{T}}$ encloses the experimental responses at the measured DOFs;

$\mathbf{X}^A(r)=\left\{\ddot{\mathbf{x}}^A(r)\ \ \dot{\mathbf{x}}^A(r)\ \ \mathbf{x}^A(r)\right\}^{\mathrm{T}}$ are the corresponding analytical counterparts; $\mathbf{W}$ is a weighting matrix, representing the uncertainty of the acceleration, velocity and displacement responses; $\beta\|r\|_1$ is the 1-norm regularization (or l_1 regularization) item to stabilize the solution of the ill-posed model updating problem; β is the regularization parameter [38].

The FE model is then iteratively adjusted to minimize the norm of the objective function $f(r)$. The sensitivity matrix of the objective function provides the searching direction of the optimization, which is expressed as

$$S(r)=\frac{\partial f(r)}{\partial r}=\mathbf{W}\frac{\partial \mathbf{X}^A(r)}{\partial r}+sign(r)\beta \tag{33}$$

where $sign(r)$ denotes the sign of r. The proposed dynamic condensation approach is used to calculate the analytical responses $\mathbf{X}^A(r)$ and response sensitivities $\frac{\partial \mathbf{X}^A(r)}{\partial r}$ at measured DOFs. The flowchart of the proposed model updating method is shown in Fig. 1. The detailed process is listed as follows:

(1) The structural responses of the FE model are calculated using the dynamic condensation approach:

a) The total DOFs are divided into master and slave ones. The matrices $\mathbf{K}_{ms}$, $\mathbf{K}_{ss}$, $\mathbf{M}_{ms}$ and $\mathbf{M}_{ss}$ are extracted from the corresponding system matrices according to the selected master and slave DOFs. The intermediate variables $\mathbf{T}_G$, $\mathbf{S}$, $\tilde{\mathbf{M}}$ and $\mathbf{K}_G$ are computed using Eqs. (11), (12), (13) and (17).

b) The transformation matrix $\mathbf{T}$ is initialized with the Guyan static condensation as $\mathbf{T}^{[0]} = \mathbf{T}_G$. In the kth iteration (k = 0, 1, 2, …), $\mathbf{M}_d$ and $\mathbf{T}$ are calculated as

$$\mathbf{M}_d^{[k]} = \mathbf{T}_G^{\mathrm{T}} \mathbf{M} \mathbf{T}^{[k]} \tag{34}$$

$$\mathbf{T}^{[k+1]} = \mathbf{T}_G + \mathbf{S}\tilde{\mathbf{M}}\mathbf{T}^{[k]} \left(\mathbf{M}_d^{[k]} \right)^{-1} \mathbf{K}_G \tag{35}$$

The iterations stop when the relative differences of the eigenvalues $\lambda^{[k]} = \mathrm{eig}\left(\left(\mathbf{M}_d^{[k]} \right)^{-1} \mathbf{K}_G \right)$ from two consecutive iterations are less than the predefined tolerance [37].

c) With the converged $\mathbf{T}^{[k+1]}$, the reduced system matrices $\mathbf{M}_R$, $\mathbf{K}_R$, $\mathbf{C}_R$ and $\mathbf{F}_R$ are formed from Eqs. (4)–(7). The structural responses at master DOFs $\ddot{\mathbf{x}}_m$, $\dot{\mathbf{x}}_m$ and $\mathbf{x}_m$ are calculated from Eq. (3) by using numerical time integration methods. The structural responses of the global model $\ddot{\mathbf{x}}$, $\dot{\mathbf{x}}$ and $\mathbf{x}$ are finally recovered from those at master DOFs by Eq. (2).

(2) The objective function is constructed with the experimental and analytical responses at the measured DOFs according to Eq. (32).

(3) The response sensitivities are computed for each design parameter r using the dynamic condensation approach. In this process, the variables obtained in the former step to compute structural responses are reused directly for efficiency. The detailed process is as follows:

a) The derivative matrices $\frac{\partial \mathbf{K}_{ms}}{\partial r}$, $\frac{\partial \mathbf{K}_{ss}}{\partial r}$, $\frac{\partial \mathbf{M}_{ms}}{\partial r}$ and $\frac{\partial \mathbf{M}_{ss}}{\partial r}$ are extracted from the corresponding elemental matrices $\frac{\partial \mathbf{K}}{\partial r}$ and $\frac{\partial \mathbf{M}}{\partial r}$ according to the selected master and slave DOFs. The intermediate derivative matrices $\frac{\partial \mathbf{T}_G}{\partial r}$, $\frac{\partial \mathbf{S}}{\partial r}$, $\frac{\partial \tilde{\mathbf{M}}}{\partial r}$ and $\frac{\partial \mathbf{K}_G}{\partial r}$ are computed according to Eqs. (27)–(30).

b) Identically, $\frac{\partial \mathbf{T}}{\partial r}$ is initialized with the Guyan static condensation as $\left[\frac{\partial \mathbf{T}}{\partial r} \right]^{[0]} = \frac{\partial \mathbf{T}_G}{\partial r}$. In

the pth iteration (p = 0, 1, 2, …),

$$\left[\frac{\partial \mathbf{M}_d}{\partial r}\right]^{[p]} = \frac{\partial \mathbf{T}_G^{\mathrm{T}}}{\partial r}\mathbf{M}\mathbf{T} + \mathbf{T}_G^{\mathrm{T}}\frac{\partial \mathbf{M}}{\partial r}\mathbf{T} + \mathbf{T}_G^{\mathrm{T}}\mathbf{M}\left[\frac{\partial \mathbf{T}}{\partial r}\right]^{[p]} \tag{36}$$

$$\left[\frac{\partial \mathbf{T}}{\partial r}\right]^{[p+1]} = \frac{\partial \mathbf{T}_G}{\partial r} + \left(\frac{\partial \mathbf{S}}{\partial r}\tilde{\mathbf{M}}\mathbf{T} + \mathbf{S}\frac{\partial \tilde{\mathbf{M}}}{\partial r}\mathbf{T} + \mathbf{S}\tilde{\mathbf{M}}\left[\frac{\partial \mathbf{T}}{\partial r}\right]^{[p]}\right)\mathbf{M}_d^{-1}\mathbf{K}_G + \mathbf{S}\tilde{\mathbf{M}}\mathbf{T}\mathbf{M}_d^{-1}\left(\frac{\partial \mathbf{K}_G}{\partial r} - \left[\frac{\partial \mathbf{M}_d}{\partial r}\right]^{[p]}\mathbf{M}_d^{-1}\mathbf{K}_G\right) \tag{37}$$

The iterations stop when the relative differences of the eigenvalues $\tilde{\lambda}^{[p]} = \mathrm{eig}\left(\left[\frac{\partial \mathbf{M}_d}{\partial r}\right]^{[p]}\mathbf{K}_G\right)$ from two consecutive iterations satisfy the predefined tolerance [37].

c) On the basis of the converged $\left[\frac{\partial \mathbf{T}}{\partial r}\right]^{[p+1]}$, the derivative matrices $\frac{\partial \mathbf{M}_R}{\partial r}$, $\frac{\partial \mathbf{K}_R}{\partial r}$, $\frac{\partial \mathbf{C}_R}{\partial r}$ and $\frac{\partial \mathbf{F}_R}{\partial r}$ are calculated from Eqs. (21)–(24). The response sensitivities at master DOFs $\frac{\partial \ddot{\mathbf{x}}_m}{\partial r}$, $\frac{\partial \dot{\mathbf{x}}_m}{\partial r}$ and $\frac{\partial \mathbf{x}_m}{\partial r}$ are calculated from Eq. (20) using numerical time integration methods. Finally, the response sensitivities at all DOFs are recovered from those at master DOFs according to Eq. (31).

(4) The sensitivity matrix of the objective function $S(r)$ is formed from Eq. (33) for each design parameter at the measured DOFs. The design parameters are then iteratively modified to minimize the objective function with optimization algorithm to achieve an accurate FE model.

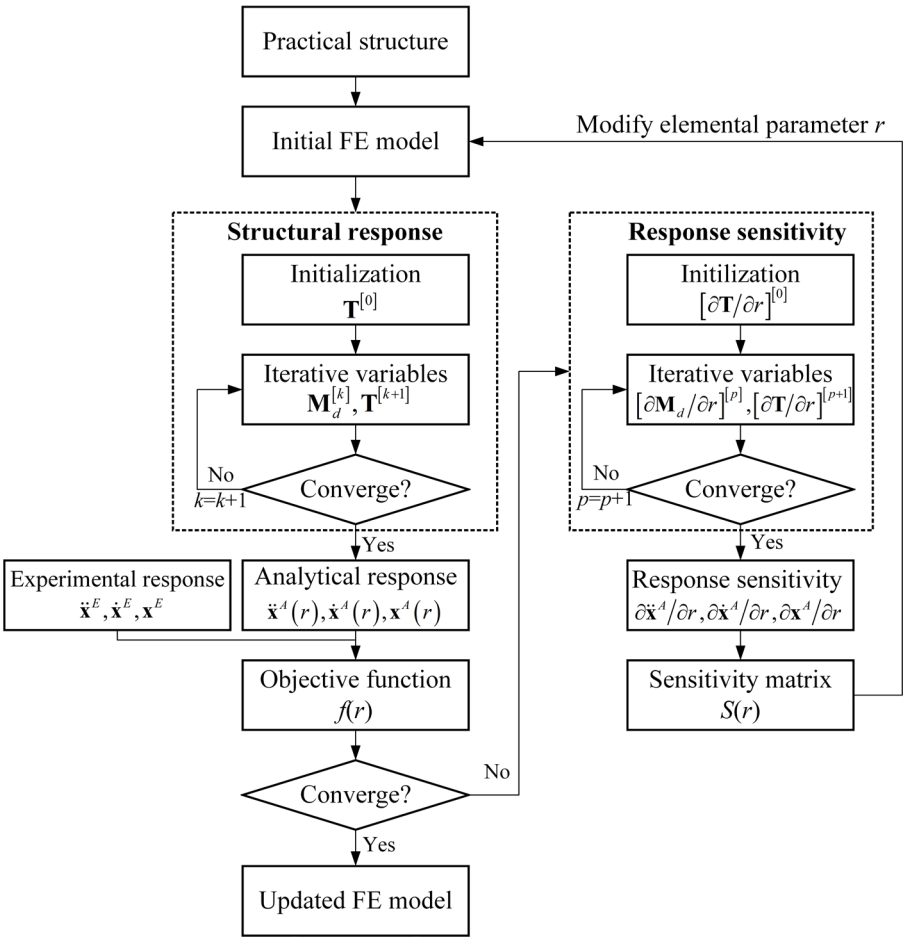

Fig. 1. Flowchart of response-based model updating using dynamic condensation approach.

The proposed model updating method is superior to the traditional global method in terms of computational efficiency and storage in two aspects. Different from the traditional method that computes the structural responses and response sensitivities from the global vibration equation (Eq. (1)) directly, the proposed method adopts the dynamic condensation approach to reduce Eq. (1) into a small-sized vibration equation. The structural responses and response sensitivities are then calculated from the reduced vibration equation, which saves considerable computational time and resources. On the other hand, the analytical responses and response sensitivities at the measured DOFs are utilized only in response-based model updating methods. The dynamic condensation approach allows the structural responses and response sensitivities

at the measured DOFs to be calculated solely in Eqs. (10) and (31), whereas the structural responses and response sensitivities at all DOFs need to be computed and stored in the global method. The accuracy and efficiency of the proposed method are verified using two numerical examples in the following sections.

4. Case study 1: nine-storey frame

A steel frame shown in Fig. 2 is firstly used to verify the accuracy of the proposed model updating method. It is modelled with 166 nodes, 189 2D Euler-Bernoulli beam elements. Each node has three DOFs, i.e., the horizontal direction u, vertical direction v and rotation θ, resulting in 486 DOFs in total. The physical parameters of each element are as follows: Young's modulus E = 200 GPa, mass density ρ = 7850 kg/m^3, cross-section of area of the columns A_{col} = 2.651×10^{-3} m^2 and the beams $A_{\text{beam}} = 5.65\times10^{-4}$ m^2 and inertial moment of the columns I_{col} = 2.578×10^{-5} m^4 and the beams $I_{\text{beam}} = 2.31\times10^{-6}$ m^4. The Rayleigh damping coefficients with respect to the mass and stiffness matrices are set to a = 0.3309 s^{-1} and $b = 5.219\times10^{-3}$ s. The structure is assumed to be excited by an El Centro earthquake wave with the peak ground acceleration of 0.4 g in the horizontal direction. As shown in Fig. 3, the wave lasts 15 seconds at a sampling rate of 200 Hz.

The structural responses and response sensitivities are firstly investigated. As shown in Fig. 2, 9 horizontal and 36 rotational DOFs are selected as master DOFs. The change ratio of the bending rigidity of Element D1 in Fig. 2 serves as the design parameter r. Three iterations are

required to ensure that $\mathbf{T}$ and $\frac{\partial \mathbf{T}}{\partial r}$ converged in the dynamic condensation approach. The calculated structural responses and response sensitivities are compared with those using the traditional global method, which computes the structural responses with the Wilson-θ method and response sensitivities with the direct differentiation method [24], based on the global vibration equation (Eq. (1)).

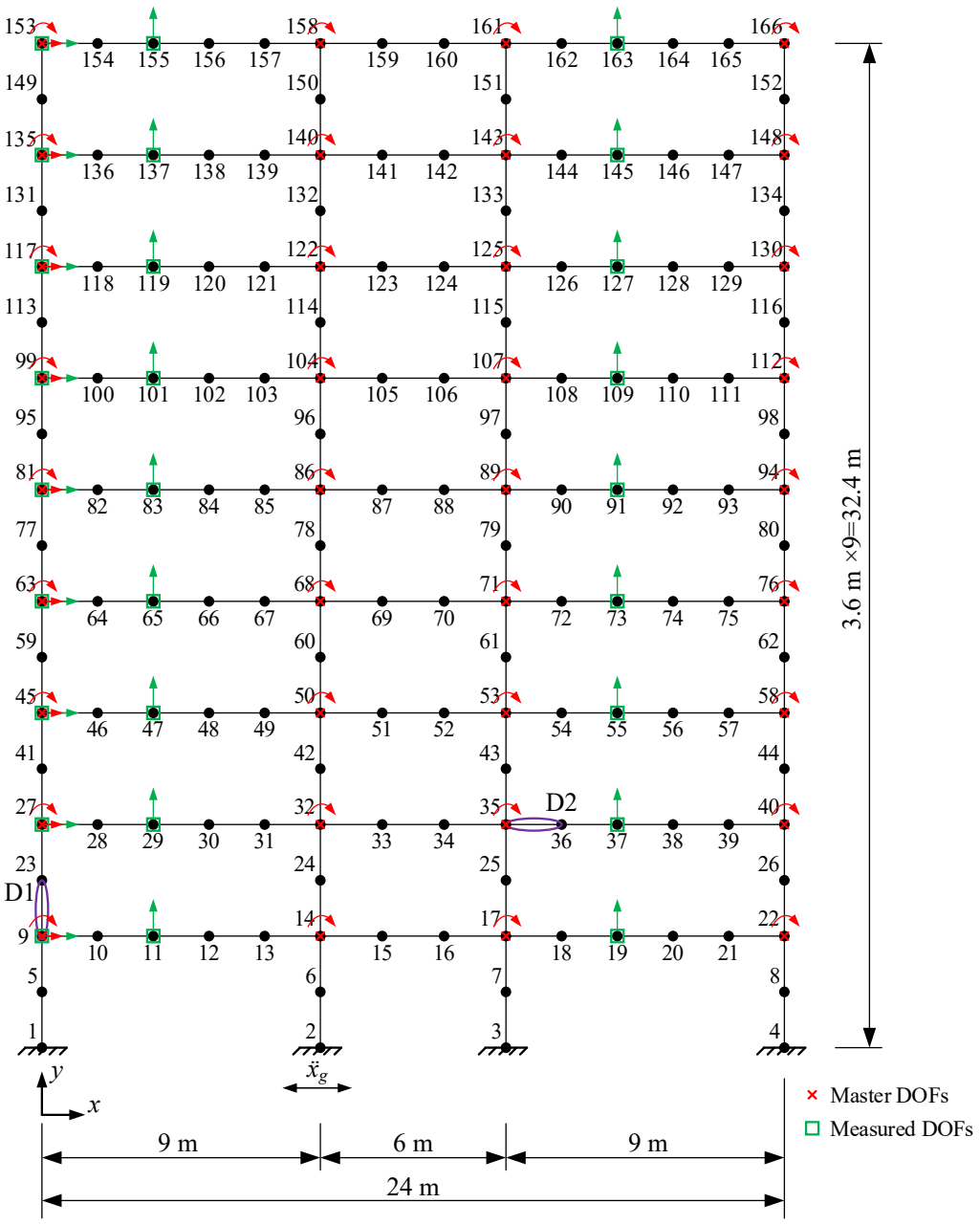

Fig. 2. Nine-storey steel frame.

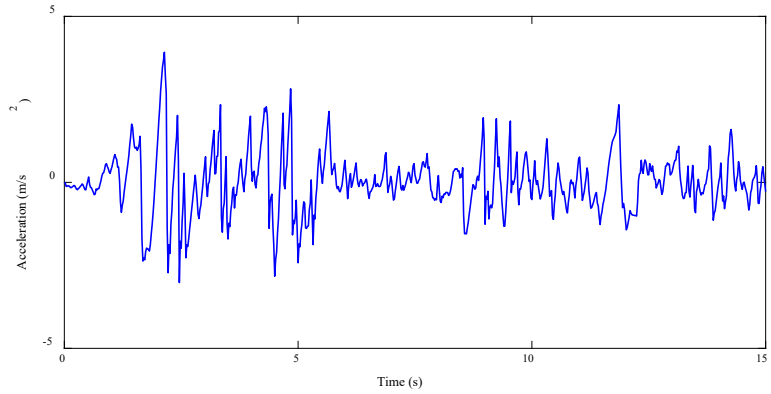

Fig. 3. El Centro earthquake wave with peak ground acceleration of 0.4 g.

Figs. 4 and 5 compare the displacement response of a randomly selected DOF (horizontal direction of Node 9) and its displacement derivative with respect to r by the two methods, respectively. The curves using the dynamic condensation approach overlap those of the global method. The relative difference of the two sets of results is calculated as

$$\text{Relative error}\left(\mathbf{X},\mathbf{Y}\right)=\left|\frac{\text{norm}\left(\mathbf{X}\right)-\text{norm}\left(\mathbf{Y}\right)}{\text{norm}\left(\mathbf{Y}\right)}\right| \tag{38}$$

where norm (·) denotes the Euclidean norm of a vector. Figs. 6 and 7 compare the relative difference of the displacement and displacement derivative with respect to r at all measured DOFs between the dynamic condensation approach and global method. The relative differences are in the order of 10^{-4} or less mostly, indicating the proposed dynamic condensation approach is very accurate in computing structural responses and response sensitivities.

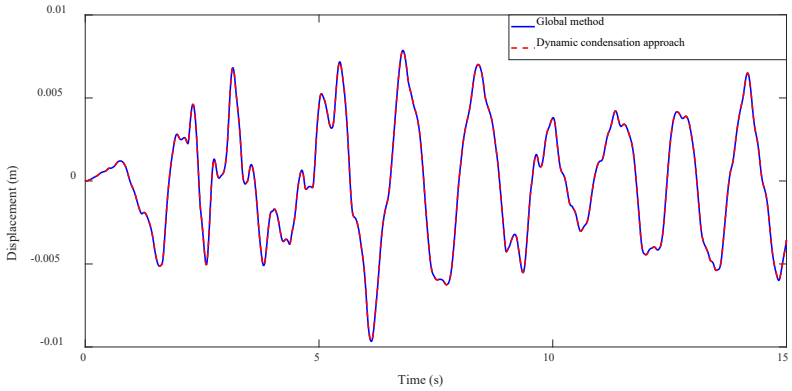

Fig. 4. Horizontal displacement of Node 9.

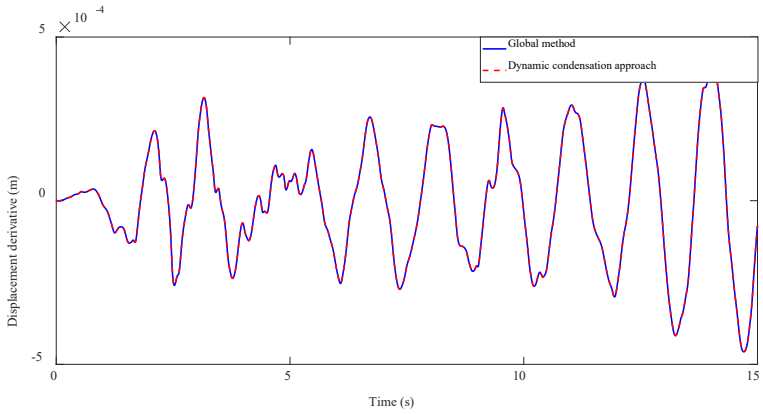

Fig. 5. Horizontal displacement derivative of Node 9 with respect to *r*.

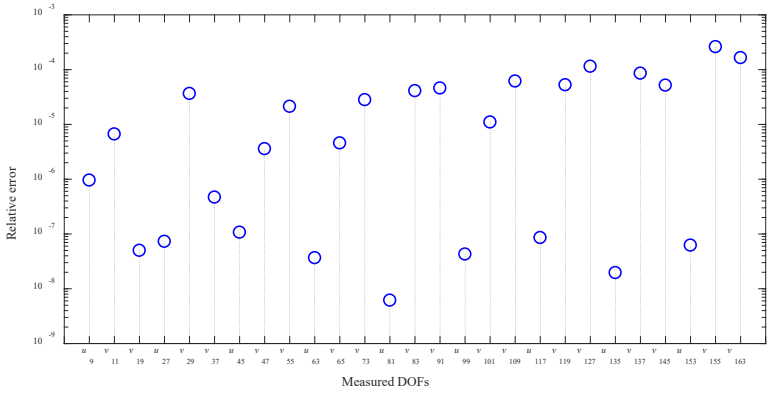

Fig. 6. Relative errors of displacement responses

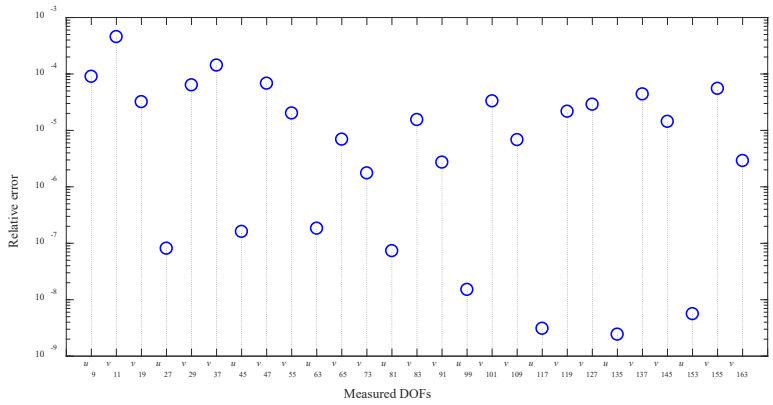

Fig. 7. Relative errors of displacement derivatives with respect to *r*.

In model updating, the FE model is iteratively adjusted to minimize the discrepancies between the experimental and analytical responses. In this example, the experimental model is simulated by the FE model with the bending rigidity of some elements intentionally reduced. Then, the proposed model updating method is implemented to identify the elemental bending rigidity reduction. A total of 27 uniformly distributed DOFs (9 horizontal DOFs and 18 vertical DOFs) are assumed to be measured, as denoted in Fig. 2. It is noteworthy that the measured DOFs are not necessarily the same as the master DOFs.

The bending rigidities of all elements are assumed to be the updating parameters, leading to 189 in total. Four cases, as listed in Table 1, are investigated. The stiffness reduction factor (SRF) is used to indicate the relative reduction in the elemental bending rigidity. In Case 1, the SRF of a randomly selected column element (Element D1) is −40%, whereas other elements remain zeros. In addition to the SRF of −40% in Element D1, the SRF of another beam element (Element D2) is −20% in Case 2. In Cases 3 and 4, the SRF of D1 is −40%, and the measurement noise is included in the responses. The measurement noise is simulated by adding

the normally distributed random noise to the true response as

$$\mathbf{x}_n^E = \mathbf{x}^E \left(1 + eR\right) \tag{39}$$

where $\mathbf{x}_n^E$ and $\mathbf{x}^E$ are the measurement response with and without noise, respectively; e is the level of noise, and R is a normally distributed random number with a mean value of zero and a unit standard deviation. 1% and 5% noises are added in Cases 3 and 4, respectively.

Table 1. Reductions in elemental bending rigidity.

Cases	Noise level	Assumed SRF
Case 1	0	Element D1 (−40%)
Case 2	0	Elements D1 (−40%) and D2 (−20%)
Case 3	1%	Element D1 (−40%)
Case 4	5%	Element D1 (−40%)

The objective function is constructed as the differences of the displacements at the measured DOFs between the analytical FE model and the simulated experimental model, that is, the weighting coefficients of the displacement responses are set to 1, and the velocity and acceleration responses are excluded in the objective function (Eq. (32)). The model updating is then performed to minimize the objective function. The optimization is performed with the trust-region-reflective algorithm in the Optimization Toolbox in Matlab platform [39, 40]. The algorithm uses the sensitivity matrix of the objective function to provide a rapid optimal searching direction. It is an effective method to handle large sparse problems. The regularization parameters are set to 0 for Cases 1 and 2 and 1×10^{-6} for Cases 3 and 4. The model updating process stops when the norm of the objective function reaches the predefined

tolerance of 1×10^{-5} m or its relative difference between two consecutive iterations are less than 1×10^{-4}. A total of 26, 40, 17 and 37 iterations are required for Cases 1–4, respectively.

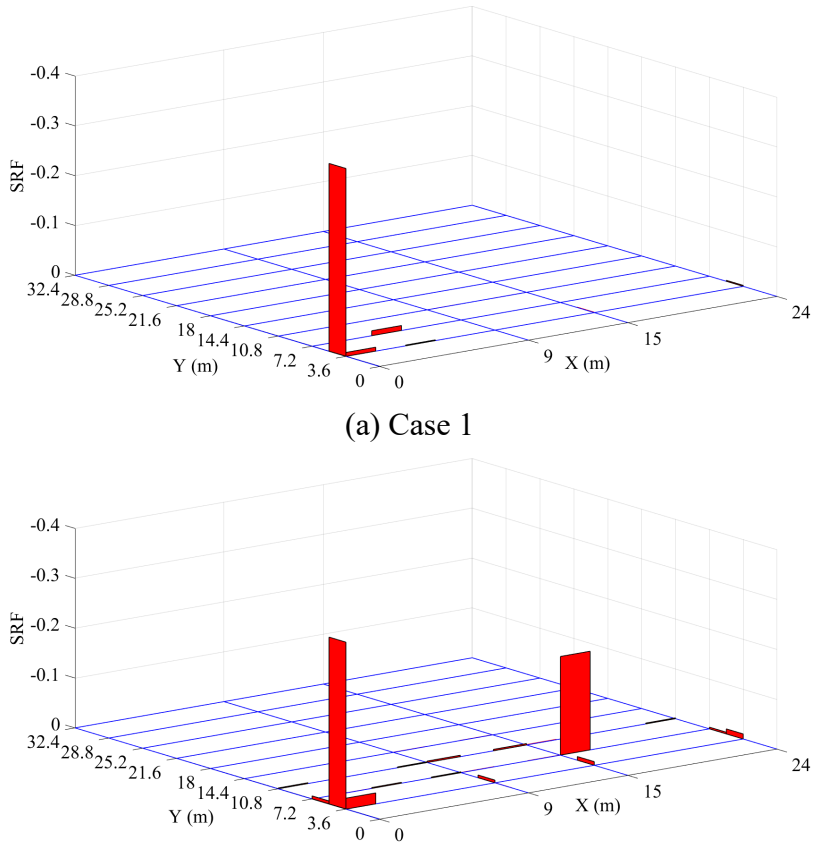

(a) Case 1

(b) Case 2

Fig. 8. Identified elemental SRFs without noise.

Fig. 8 displays the identified SRF of Cases 1 and 2. In both cases, the actual stiffness reduction can be accurately identified with minor errors in other unchanged elements, thereby implying that the proposed method is very accurate for model updating.

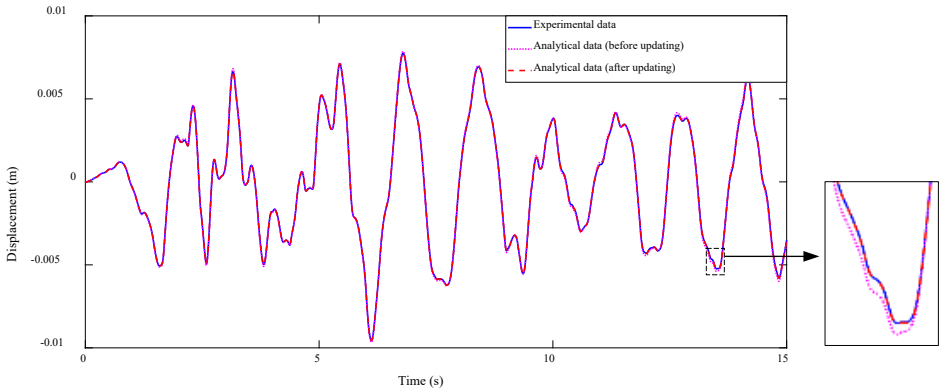

(a) Case 1

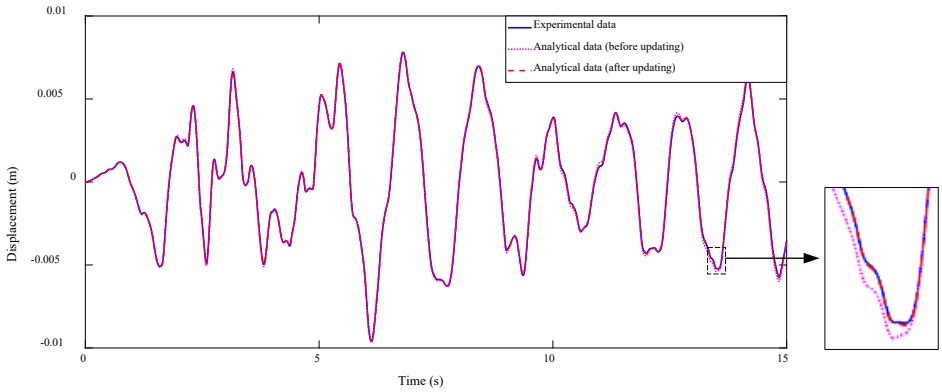

(b) Case 2

Fig. 9. Horizontal displacement of Node 9 before and after model updating.

Fig. 9 compares the horizontal displacement of Node 9 before and after updating for Cases 1 and 2. The analytical responses moderately deviate from the experimental ones before updating. After model updating, the two curves are in good agreement. Fig. 10 displays the relative errors between the analytical displacement responses and the experimental counterparts at all measured DOFs. The relative errors decrease significantly after the model updating is performed. This verifies again that the proposed method is very accurate for model updating.

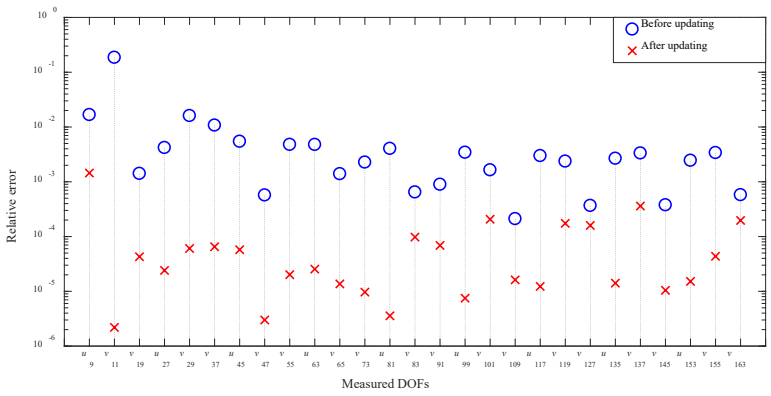

(a) Case 1

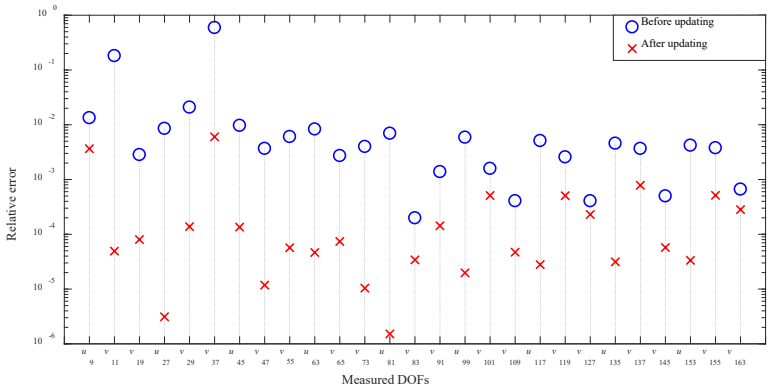

(b) Case 2

Fig. 10. Relative errors of the analytical responses before and after model updating.

Fig. 11 shows the identified SRFs of Cases 3 and 4. When 1% measurement noise is considered (Case 3), an evident stiffness reduction is identified in Element D1 with minor errors in other unchanged elements. As the measurement noise increases to 5% (Case 4), the actual reduced elements can be identified with some small SRFs identified in the unchanged elements. Therefore, the proposed model updating method has good robustness of measurement noise.

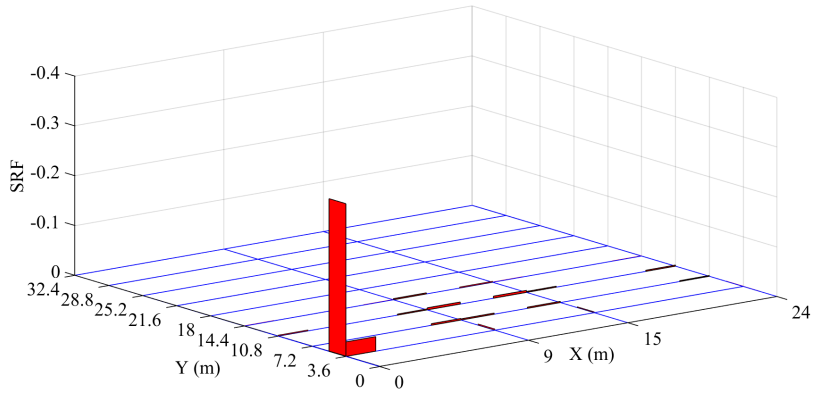

(a) Case 3 (1% noise)

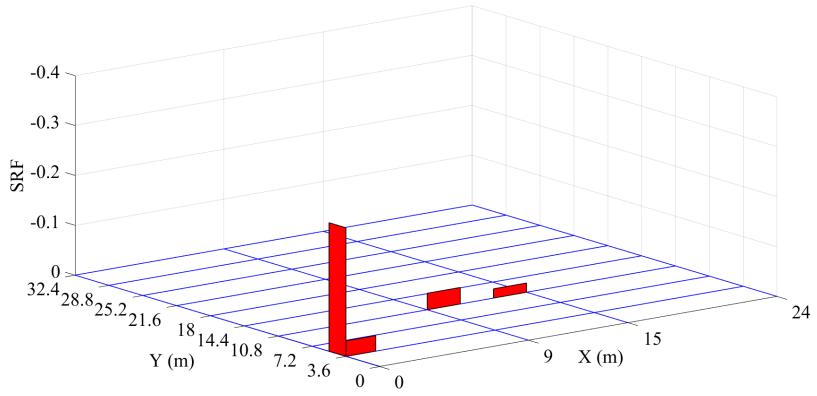

(b) Case 4 (5% noise)

Fig. 11. Identified elemental SRFs under different levels of noise.

5. Case study 2: suspension bridge

A practical suspension bridge, Jiangyin Yangtze River Bridge in Jiangsu Province, China, is used to investigate the efficiency of the proposed model updating method for large-scale structures. The bridge has a main span of 1385 m [41]. It has two pylons of 184 m and 187 m high. The steel box girder is 32.5 m wide and 3 m high. A simplified FE model, as shown in Fig. 12, is constructed from the design drawings of the bridge. The side spans are independent on the main span and thus excluded in the FE model. The model is composed of 653 nodes, 826 elements and 3178 DOFs. The Rayleigh damping coefficients associated with the mass

and stiffness matrices are set to $a = 0.3309\ \mathrm{s}^{-1}$ and $b = 5.219\times10^{-3}$ s, respectively. The El Centro earthquake wave with a peak ground acceleration of 0.1 g is applied to the Y direction of the structure. The earthquake wave, as shown in Fig. 13, lasts 15 seconds with a sampling rate of 200 Hz. Using the dynamic condensation approach, nine uniformly distributed nodes on the girder (Fig. 12) are selected as the master nodes. Each node has three master DOFs, i.e., X-, Y- and Z-directions, resulting in 27 master DOFs in total. Three iterations are required to ensure the convergence of $\mathbf{T}$ and $\frac{\partial \mathbf{T}}{\partial r}$.

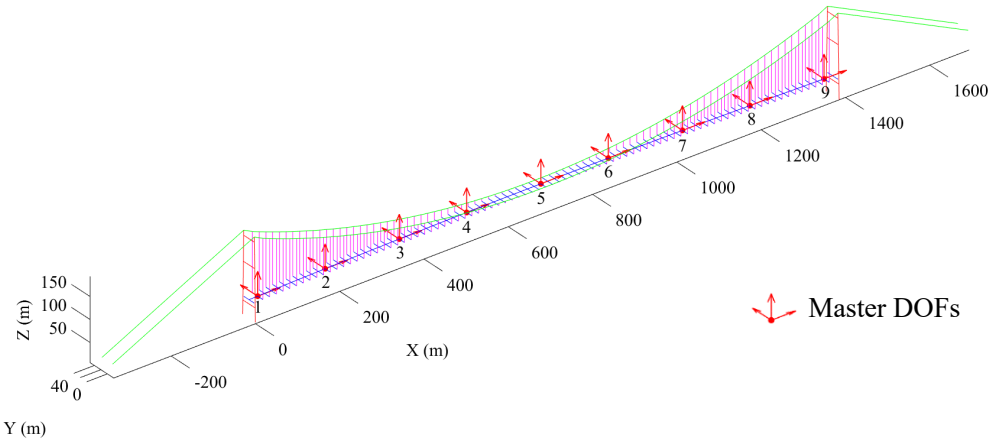

Fig. 12. FE model of Jiangyin Bridge.

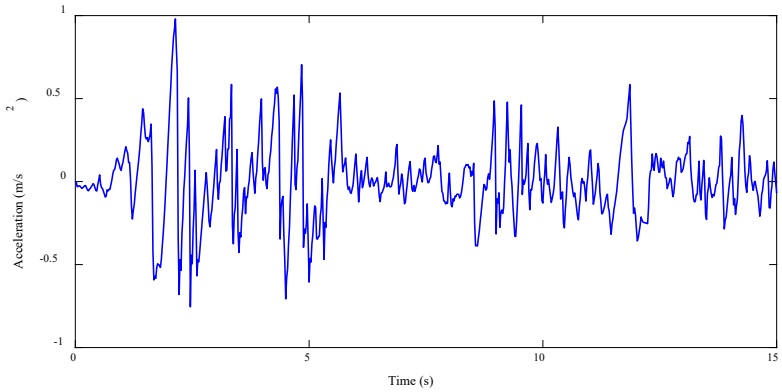

Fig. 13. El Centro earthquake wave with peak ground acceleration of 0.1 g.

The FE model is simulated by intentionally changing the bending rigidity of some elements. In

this case, the bending rigidity of all girder elements is assumed to be randomly changed by −50%~50%. The bridge responses are then calculated from the FE model. The displacements of the master nodes in the Y direction are assumed as the measured data, yielding nine measured DOFs in total. The measured DOFs are included in the master DOFs; thus, only the responses and response sensitivities at the 27 master DOFs need to be computed and stored. The objective function is constructed with the differences between the measured displacement and the model predictions. The SRFs of all girder elements are selected as updating parameters. Consequently, the total updating parameter is 260.

Model updating is performed on the Matlab Optimization Toolbox in an ordinary desktop computer with 3.60 GHz CPU and 20 GB RAM. The model updating process stops when the norm of the objective function reaches the predefined tolerance of 1×10^{-3} m. The regularization parameter is set to zero. Again, the global model updating method is used as a reference. The convergence process of the two model updating methods in terms of the norm of the objective function is shown in Fig. 14. The computational time and number of iterations of the two methods are compared in Table 2.

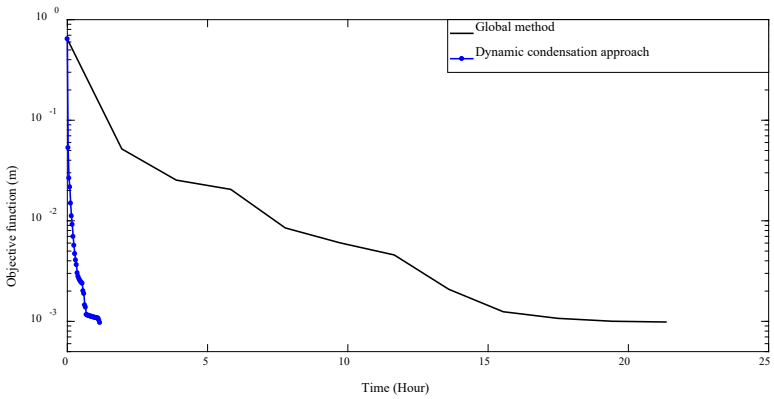

Fig. 14. Convergence of the two model updating methods.

Table 2. Computational time and number of iterations.

Methods	Time for each iteration (Hour)	Number of iterations	Total time (Hour)	Relative ratio
Dynamic condensation approach	0.0297	39	1.16	5.43%
Global method	1.942	11	21.36	100.00%

The global method requires 1.942 hours for each iteration and 21.36 hours in total for the entire model updating process. Using the dynamic condensation approach, however, each iteration requires 0.0297 hours only and the model updating process stops after 39 iterations within 1.942 hours, accounting for 5.43% of the global method. The computational efficiency of the proposed model updating is improved greatly. This is because only 27 master DOFs are used in the dynamic condensation approach, resulting in the reduced system matrices with the size of 27×27, much smaller than the global ones with 3178×3178. Although more iterations are required in the proposed method, the total computational time is saved remarkably. Fig. 15 compares the displacement of a randomly selected measured DOF (master node 5 in the Y direction). The analytical displacement deviates significantly from the experimental one before model updating. The two curves are overlapped after the proposed model updating is implemented. Fig. 16 compares the relative errors of the analytical responses at all measured DOFs before and after model updating. The relative errors are reduced significantly from approximately 10^{-1} to 10^{-3} after the model updating is conducted. Therefore, the proposed method is very accurate and efficient to update the FE model of large-scale structures with only a few master DOFs and measured time history responses.

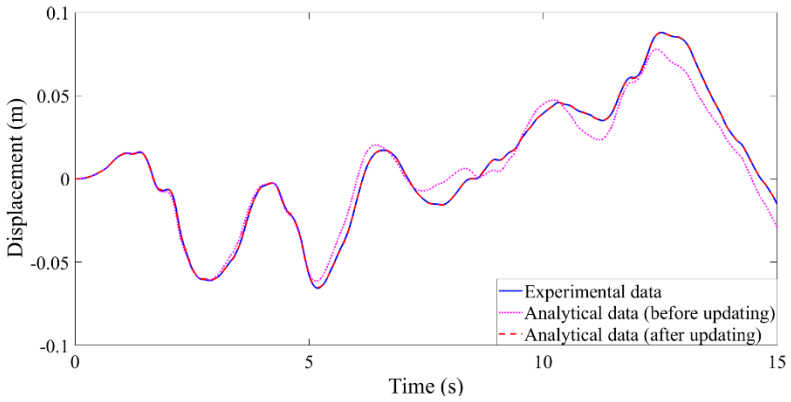

Fig. 15. Displacement of Node 5 in Y direction before and after model updating.

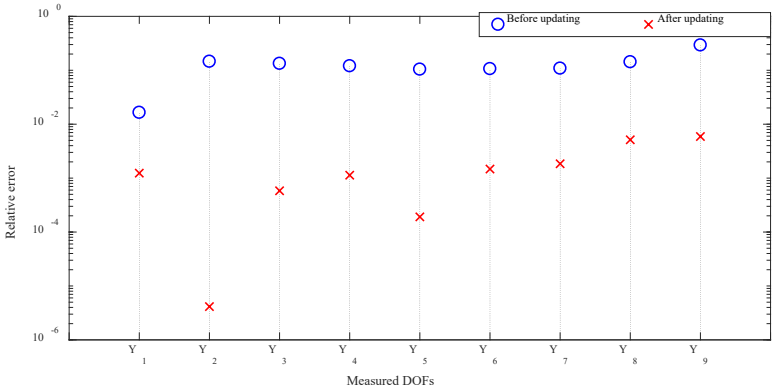

Fig. 16. Relative errors of the analytical responses before and after model updating.

6. Conclusions

A dynamic condensation approach is developed for accurate and efficient response-based FE model updating of large-scale structures. The large-size vibration equation of the global model is reduced into a much smaller one according to the selected master DOFs. The structural responses are then computed efficiently from the reduced vibration equation. The response sensitivities are calculated simultaneously and efficiently by taking the derivative of the reduced vibration equation with respect to the design parameters directly without additional master DOFs. The FE model updating is then implemented using the time history responses

and response sensitivities at a few measurement points only. Applications to two numerical examples demonstrate that the proposed method is accurate and efficient for response-based model updating of large-scale structures.

Acknowledgements

The work described in this paper is supported by the Key Area R&D Program of Guangdong Province (Project No. 2019B111106001), National Key R&D Program (Project No. 2019YFB1600700) and National Natural Science Foundation of China (NSFC, 51778258, 51922046).

References

[1] L. Dai, Finite-element model updating of the traditional beam-column joint in Tibetan heritage buildings using uniform design, Adv. Struct. Eng. 23 (9) (2020) 1890-1901.

[2] S. Weng, H.P. Zhu, Y. Xia, J.J. Li, W. Tian, A review on dynamic substructuring methods for model updating and damage detection of large-scale structures, Adv. Struct. Eng. 23 (3) (2020) 584-600.

[3] R.R. Hou, Y. Xia, Review on the new development of vibration-based damage identification for civil engineering structures: 2010-2019, J. Sound Vib. 491 (2021) 115741.

[4] R. Rocchetta, M. Broggi, Q. Huchet, E. Patelli, On-line Bayesian model updating for structural health monitoring, Mech. Syst. Signal Process. 103 (2018) 174-195.

[5] J.E. Mottershead, M. Link, M.I. Friswell, The sensitivity method in finite element model updating: a tutorial, Mech. Syst. Signal Process. 25 (2011) 2275-2296.

[6] S.A. Dunn, The use of genetic algorithms and stochastic hill-climbing in dynamic finite element model identification, Comput. Struct. 66 (1998) 489-497.

[7] H. Hao, Y. Xia, Vibration-based damage detection of structures by genetic algorithm, J. Comput. Civil Eng. 16 (3) (2002) 222-229.

[8] S. Tiachacht, A. Bouazzouni, S. Khatir, M.A. Wahab, A. Behtani, R. Capozucca, Damage assessment in structures using combination of a modified Cornwell indicator and genetic algorithm, Eng. Struct. 177 (2018) 421-430.

[9] H. Tran-Ngoc, S. Khatir, G. De Roeck, T. Bui-Tien, L. Nguyen-Ngoc, M.A. Wahab, Model updating for Nam O Bridge using particle swarm optimization algorithm and genetic algorithm, Sensors. 18 (2018) 4131.

[10] H. Tran-Ngoc, S. Khatir, G. De Roeck, T. Bui-Tien, M.A. Wahab, An efficient artificial neural network for damage detection in bridges and beam-like structures by improving training parameters using cuckoo search algorithm, Eng. Struct. 199 (2019) 109637.

[11] R.R. Hou, Y. Xia, X.Q. Zhou, (2019), Genetic algorithm based optimal sensor placement for L_1-regularized damage detection, Struct. Control Hlth. 26 (1) (2019) e2274.

[12] H. Tran-Ngoc, L.Q. He, E. Reynders, S. Khatir, T. Le-Xuan, G. De Roeck, T. Bui-Tien,

M.A. Wahab, An efficient approach to model updating for a multispan railway bridge using orthogonal diagonalization combined with improved particle swarm optimization, J. Sound Vib. 476 (2020) 115315.

[13] N. Cottin, J. Reetz, Accuracy of multiparameter eigenvalues used for dynamic model updating with measured natural frequencies only, Mech. Syst. Signal Process. 20 (1) (2006) 65-77.

[14] Y.X. Wu, J. Zhong, C. Conti, P. Dehombreux, Quasi-mode shape based dynamic finite element model updating method, J. Mater. Process. Tech. 138 (2003) 518-521.

[15] J. Niu, Z.H. Zong, F.P. Chu, Damage identification method of girder bridges based on finite element model updating and modal strain energy, Sci. China-Technol. Sc. 58 (4) (2015) 701-711.

[16] B. Jaishi, W.X. Ren, Damage detection by finite element model updating using modal flexibility residual, J. Sound Vib. 290 (1-2) (2006) 369-387.

[17] N. Guo, Z.C. Yang, L. Wang, Y. Ouyang, X.P. Zhang, Dynamic model updating based on strain mode shape and natural frequency using hybrid pattern search technique, J. Sound Vib. 422 (2018) 112-130.

[18] A. Esfandiari, F. Bakhtiari-Nejad, M. Sanayei, A. Rahai, Structural finite element model updating using transfer function data, Comput. Struct. 88 (1-2) (2010) 54-64.

[19] M. Link, M. Weiland, Damage identification by multi-model updating in the modal and in the time domain, Mech. Syst. Signal Process. 23 (6) (2009) 1734-1746.

[20] Y.Z. Fu, Z.R. Lu, J.K. Liu, Damage identification in plates using finite element model updating in time domain, J. Sound Vib. 332 (26) (2013) 7018-7032.

[21] C. Grossmann, H.G. Roos, M. Stynes, Numerical treatment of partial differential equations, Springer, 2007.

[22] R. Kiran, L. Li, K. Khandelwal, Complex perturbation method for sensitivity analysis of nonlinear trusses, J. Struct. Eng.143 (1) (2017) 04016154.

[23] A.A. Nejat, A. Moghadasi, A. Held, Adjoint sensitivity analysis of flexible multibody systems in differential-algebraic form, Comput. Struct. 228 (2020) 106148.

[24] Q. Gu, L. Wang, Y. Li, X. Deng, C. Lin, Multi-scale response sensitivity analysis based on direct differentiation method for concrete structures, Compos. Part B-Eng. 157 (2019)

295-304.

[25] R.J. Guyan, Reduction of stiffness and mass matrices, AIAA J. 3 (2) (1965) 380.

[26] M.I Friswell, S.D. Garvey, J.E.T. Penny, Model reduction using dynamic and iterated IRS techniques, J. Sound Vib. 186 (2) (1995) 311-323.

[27] M.I. Friswell, S.D. Garvey, J.E.T. Penny, The convergence of the iterated IRS method, J. Sound Vib. 211 (1) (1998) 123-132.

[28] Y. Xia, R.M. Lin, Improvement on the iterated IRS method for structural eigensolutions, J. Sound Vib. 270 (4-5) (2004) 713-727.

[29] Y. Xia, R.M. Lin, A new iterative order reduction (IOR) method for eigensolutions of large structures, Int. J. Numer. Meth. Eng. 59 (1) (2004) 153-172.

[30] H.A. Qu, P. Selvam, Model order reduction of viscously damped vibration systems using accelerated iterative dynamic condensation, J. Appl. Mech-T. ASME. 72 (5) (2005) 761-771.

[31] A.M.G. de Lima, N. Bouhaddi, D.A. Rade, M. Belonsi, A time-domain finite element model reduction method for viscoelastic linear and nonlinear systems, Lat. Am. J. Solids Stru. 12 (6) (2015) 1182-1201.

[32] J.F. Mercer, G.S. Aglietti, A.M. Kiley, Model reduction and sensor placement methods for finite element model correlation, AIAA J. 54 (12) (2016) 3941-3955.

[33] J.H. Kim, S.H. Boo, P.S. Lee, A dynamic condensation method with free interface substructuring, Mech. Syst. Signal Process. 129 (2019), 218-234.

[34] J. Jeong, S. Baek, M. Cho, Dynamic condensation in a damped system through rational selection of primary degrees of freedom, J. Sound Vib. 331 (7) (2012) 1655-1668.

[35] T. Yin, H.P. Zhu, Selection of masters in dynamic reduction-based structural health monitoring using Bayesian experimental design, Mech. Syst. Signal Process. 150 (2021) 107294.

[36] S. Weng, A.Z. Zhu, H.P. Zhu, Y. Xia, L. Mao, P.H. Li, Dynamic condensation approach to the calculation of eigensensitivity, Comput. Struct.132 (2014) 55-64.

[37] S. Weng, W. Tian, H.P. Zhu, Y. Xia, F. Gao, Y.T. Zhang, J.J. Li., Dynamic condensation approach to calculation of structural responses and response sensitivities, Mech. Syst. Signal Process. 88 (2017) 302-317.

[38] R.R. Hou, Y. Xia, Y.Q. Bao, X.Q. Zhou, Selection of regularization parameter for l_1-regularized damage detection, J. Sound Vib. 423 (2018) 141-160.

[39] T.F. Coleman, Y. Li, An interior, trust region approach for nonlinear minimization subject to bounds, SIAM J. Optimiz. 6 (1996) 418-445.

[40] T.F. Coleman, Y. Li, On the convergence of reflective Newton methods for large-scale nonlinear minimization subject to bounds, Math. Program. 67 (2) (1994) 189-224.

[41] Q. Xia, Y. Xia, H.P. Wan, J. Zhang, W.X. Ren, Condition analysis of expansion joints of a long-span suspension bridge through metamodel-based model updating considering thermal effect, Struct. Control Health Monit. 27 (5) (2020) e2521.